Bull. Mater. Sci., Vol. 37, No. 7, December 2014, pp. 1657–1662. © Indian Academy of Sciences.

Bipolar resistive switching behaviours in $ZnMn_2O_4$ film deposited on p^+-Si substrate by chemical solution deposition

JIWEN XU[1,2,*], ZUPEI YANG[1], YUPEI ZHANG[2], XIAOWEN ZHANG[2] and HUA WANG[2]

[1]School of Material Science and Engineering, Shaanxi Normal University, Xi'an 710062, P R China

[2]School of Material Science and Engineering, Guilin University of Electronic Technology, Guilin 541004, P R China

MS received 4 January 2014; revised 24 March 2014

Abstract. **$ZnMn_2O_4$ active layer for resistance random access memory (RRAM) was deposited on p^+-Si substrate by chemical solution deposition. The bipolar resistive switching behaviours of the Ag/$ZnMn_2O_4$/p^+-Si capacitor are investigated. The bipolar resistive switching is reproducible and shows high ON/OFF ratio of $>10^2$ and long retention times of $>10^5$ s. The conduction mechanism of the Ag/$ZnMn_2O_4$/p^+-Si capacitor in the low-resistance state (LRS) is ohmic conduction, whereas that of the device in high-resistance state (HRS) successively undergoes Ohm's law, trap-filled-limited and Child's law conduction procedure at room temperature.**

Keywords. **$ZnMn_2O_4$; bipolar; resistive switching; chemical solution deposition.**

1. Introduction

Non-volatile memories (NVMs) based on resistive switching between two-terminal electrodes induced by an external electric field were first proposed by Chua (1971). In storage operation, an external voltage switches the resistance reversibly between high resistance state (HRS) and low resistance state (LRS) to realize the storage of binary code of '1' and '0'. Depending on the external voltage polarity, the resistive switching behaviour is classified as unipolar and bipolar (Waser and Aono 2007). Resistance random access memories (RRAM) are considered as one of the most promising candidates for the next generation NVMs. Resistive switching in a lot of material systems, such as binary transition metal oxides (Villafuerte *et al* 2007; Liu *et al* 2008; Yu *et al* 2008; Hou *et al* 2011), perovskites (Liu *et al* 2000; Lin *et al* 2011) and chalcogenides (Waser and Aono 2007; Pradel *et al* 2011), has attracted increasingly wide attention because of its potential applications in RRAM devices. ZnO and Mn doped ZnO as resistive switching active materials demonstrate bipolar resistive switching characteristics (Villafuerte *et al* 2007; Yang *et al* 2009; Chang *et al* 2010). The Mn–Zn–O ternary system is interesting in terms of both the electrical and magnetic properties. However, the switching behaviours in Mn–Zn–O ternary oxides have been less investigated compared with the binary counterparts. The most recent work reported by Peng and Wu (2009) states that the Au/Mn–Zn–O/Pt devices based on spinel $ZnMn_2O_4$ and ilmenite $ZnMnO_3$ active layer show unipolar resistive switching characteristics. Therefore, $ZnMn_2O_4$-based RRAM with new structure and resistive switching behaviour should be interesting.

In this work, the spinel $ZnMn_2O_4$ films were deposited on p^+-Si substrate by chemical solution method, and the Ag/$ZnMn_2O_4$/p^+-Si memory devices show bipolar resistive switching behaviour. The resistive switching characteristics and associated conduction mechanisms were also discussed in detail.

2. Experimental

The $ZnMn_2O_4$ active layer was deposited on p^+-Si substrate by chemical solution deposition. $Zn(CH_3COO)_2{\cdot}2H_2O$, $Mn(CH_3COO)_2{\cdot}4H_2O$, 2-methoxyethanol and diethanolamine were used as the starting materials, solvent and stabilizer, respectively. The 0·4 mol/L precursor was synthesized by magnetic stirring at 60 °C. The $ZnMn_2O_4$ film was deposited by multiple spin coating at 4000 rpm for 30 s, and each layer was heated at 300 °C for 15 min to remove organics. Finally, the film was annealed at 650 °C for one hour in air ambient. In order to fabricate the Ag/$ZnMn_2O_4$/p^+-Si device, the top silver electrodes of ϕ0·4 mm were deposited by thermal evaporation using a stainless steel mask.

The crystalline phase was determined by X-ray diffraction with Cu K_α radiation (XRD, Bruker D8-ADVANCE). The surface and cross-section morphologies of the annealed $ZnMn_2O_4$ film were observed by scanning electron microscope (SEM, Hitachi S4800). The resistive switching characteristics were measured by Keithley 2400 digital source meter at room temperature. A compliance current of 30 mA was used to prevent permanent breakdown of the devices. In order to investigate fatigue property, the device was stimulated repeatedly by current-voltage sweep.

*Author for correspondence (csuxjw@126.com)

3. Results and discussion

The X-ray diffraction pattern of the $ZnMn_2O_4$ film deposited on p^+-Si substrate is shown in figure 1. It can be seen that the diffraction peaks of the $ZnMn_2O_4$ film corresponds to the standard diffraction peaks (JCPDS file 71-2499), which confirms the formation of spinel phase. A strong silicon diffraction peak originating from the p^+-Si substrate can also be seen in the diffraction pattern.

SEM images in figure 2 clearly show the surface and cross-section morphologies of the $ZnMn_2O_4$ film. It can be seen that the $ZnMn_2O_4$ film shows dense and crystallized structure, which consists of numerous tiny spherical grains. The size of these tiny grains is in the range of 30–90 nm. The thickness of the $ZnMn_2O_4$ film is about 400 nm by measuring the height of the cross-section in figure 2(b).

Figure 3 shows the typical current–voltage (I–V) characteristic of the Ag/$ZnMn_2O_4$/p^+-Si device, which was measured by sweeping the bias voltage of the top electrode in the sequence of $0 \rightarrow V_{max} \rightarrow 0 \rightarrow -V_{max} \rightarrow 0$ V. The schematic illustration of the device and resistive switching measurement is depicted by the inset in figure 3. The distinct I–V hysteresis loop indicates that the device shows large resistive switching behaviour. When the external dc voltage applied to the Ag electrode is swept from 0 to 10 V, the resistance decreases dramatically at about 9 V, which indicates the resistance state changes from HRS to LRS. The device maintains the LRS while the external dc voltage is swept from 10 to 0 V. However, the resistance increases sharply at −10 V when the dc voltage is swept from 0 to −10 V. This change indicates the device changes back from LRS to HRS. The change between HRS and LRS indicates that bipolar resistive switching behaviour exists in the Ag/$ZnMn_2O_4$/p^+-Si device.

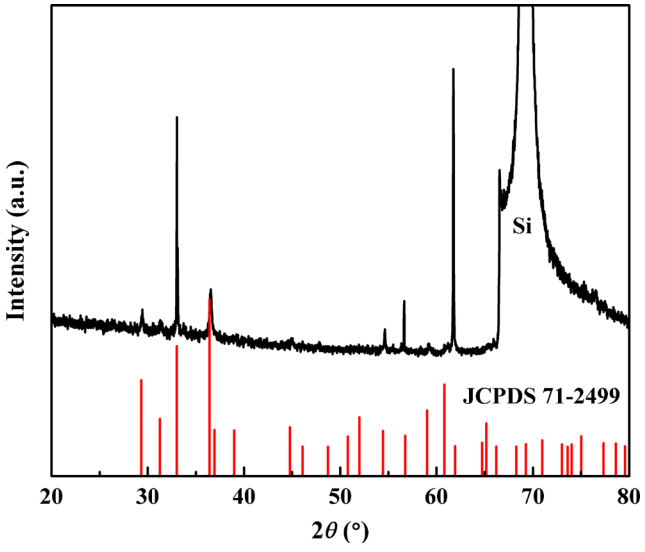

Figure 1. XRD pattern of the $ZnMn_2O_4$ film with top silver electrodes.

Report in the literature (Peng and Wu 2009) showed that the filamentary conduction and space-charge-limited conduction (SCLC) are the main mechanisms for LRS and HRS in the unipolar RRAM based on the Au/$ZnMn_2O_4$/Pt capacitors. The I–V curves are fitted to investigate the carrier transport mechanisms of the Ag/$ZnMn_2O_4$/p^+-Si capacitor in this work. The fitting data and experimental results are shown in figure 4. The I–V relationship in the LRS clearly exhibits an Ohmic conduction behaviour with a slope of 1·15, which is regarded as the formation of conductive filaments (oxygen vacancies) in the device during the set process. The LRS has densely populated filaments, which result in a low resistance. At the reset process, these conductive filaments should be destroyed by Joule heating. This model is often invoked to explain the conduction mechanism in an oxide of zinc or manganese such as ZnO, Mn-doped ZnO and MnO_x (Yang *et al* 2009; Zhang *et al* 2009; Chang *et al* 2010). However, the conduction mechanism in the HRS is more complicated than that of the LRS. Experimental results show that the three regions are clearly distinguishable in figure 4. These regions are denoted by I, II and III, which correspond to the Ohm's law, trap-filled-limited and Child's law, respectively. The current–density–voltage (J–V) characteristics in the $\log J - \log V$ plane are bounded by the three limited curves, namely, Ohm's law ($J \propto V$), Child's law ($J \propto V^2$), and trap-filled-limit (TFL) curve. The J–V equations of

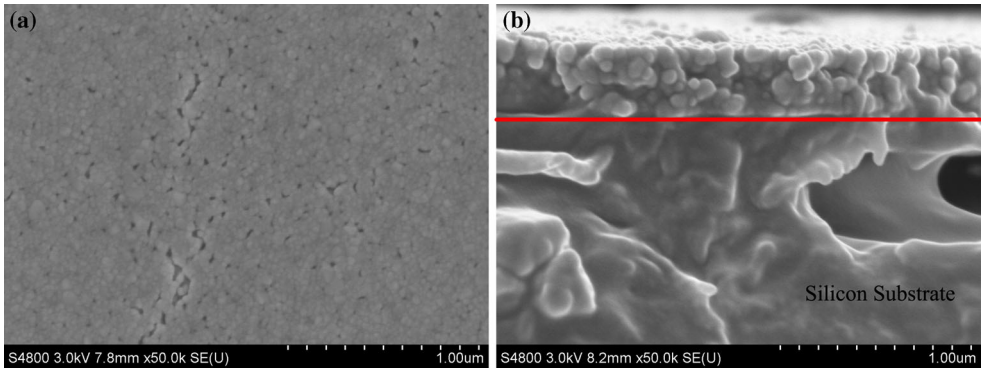

Figure 2. (**a**) Surface and (**b**) cross-section SEM images of the annealed film.

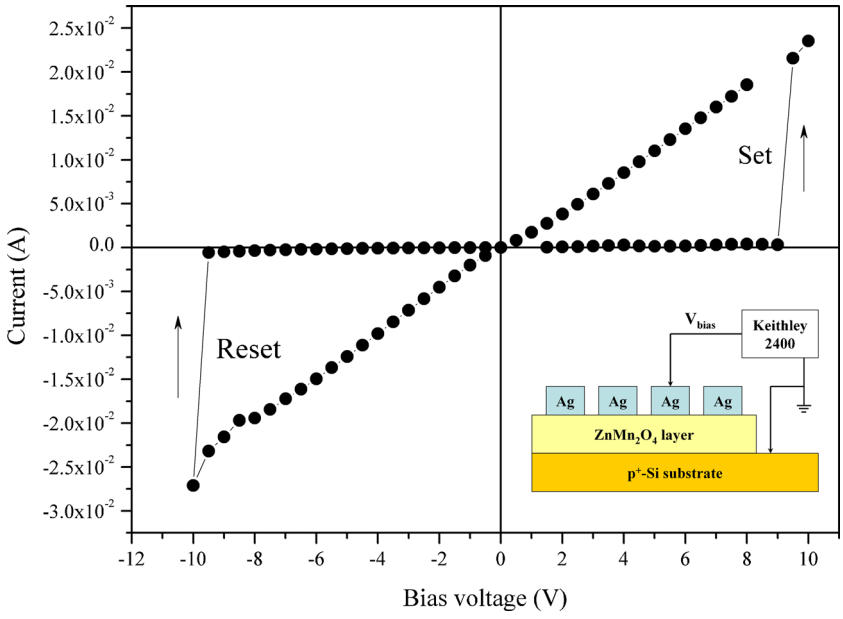

Figure 3. Bipolar resistive switching characteristic of the Ag/$ZnMn_2O_4$/p^+-Si device.

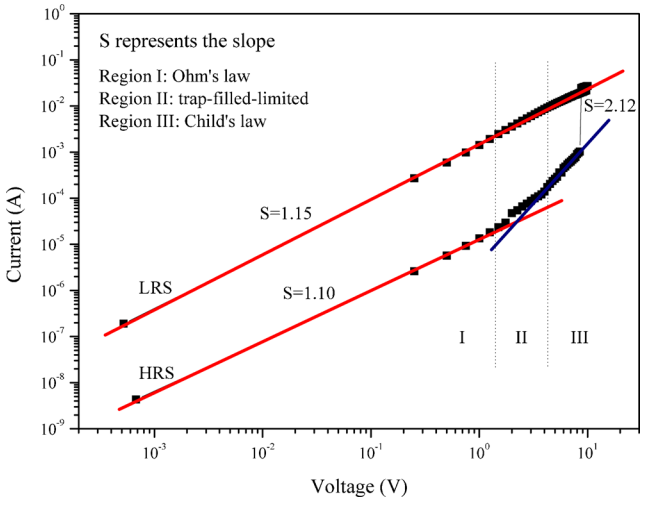

Figure 4. The typical *I–V* curves plotted in double logarithmic scale in positive sweeping voltage.

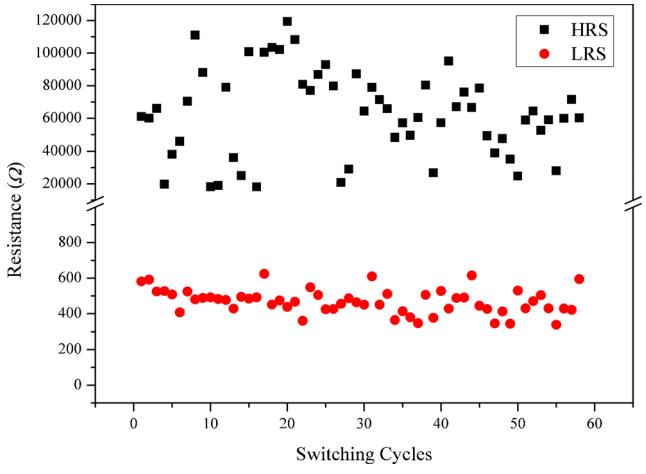

Figure 5. The endurance characteristic of the Ag/$ZnMn_2O_4$/p^+-Si device.

space-charge-limited conduction to describe the leakage current are as follows:

$$J_{\text{Ohm}} = qn_0\mu\frac{V}{d}, \tag{1}$$

$$J_{\text{TFL}} = B\left(\frac{V^{l+1}}{d^{2l+1}}\right), \tag{2}$$

$$J_{\text{Child}} = \frac{9}{8}\mu\varepsilon\frac{V^2}{d^3}, \tag{3}$$

where q is electronic charge, n_0 the concentration of the free charge carriers in thermal equilibrium, μ the electronic mobility in $ZnMn_2O_4$ films, V the applied voltage, d the thickness of film, ε the dielectric constant of $ZnMn_2O_4$, B an l-dependent parameter, $l = (T_C/T)$, T_C a characteristic temperature related to the trap distribution, and T the absolute temperature (Chiu *et al* 2005).

In region I, when the electric field across the device is small and the number of the thermally generated free electrons exceeds the injected electrons by the electric field, the current depends on the applied external field and the material conductivity. The slope of 1·10 is almost equal to one, which indicates that the *I–V* characteristics follow Ohm's law. While the injected electrons keep on increasing as the electric

field increases, the probability of injected electrons getting captured by the traps in the $ZnMn_2O_4$ film increases as well. One part of injected electrons are trapped (injected trapped electrons), and others donate to the total current (injected free electrons). This region (region II) is recognized as the charge injection limited and trap filling region. With further increasing the electric field, the trapping centres will be fully filled by a large number of injected electrons from the Ag electrode, and the current enters into region III. Moreover, the $ZnMn_2O_4$ material cannot provide the excess electrons, and thereby the space charge begins to produce near the injecting electrode interface. Therefore, space charge should start to hinder further electron injection, and extra injected electrons cannot move to the bottom electrode. At the voltage of V_{set}, filament chains consisting of substantial oxygen vacancies make the HRS change into LRS. This model is also adopted to analyse HRS conduction behaviour for the RRAM devices based on other material systems such as TiO_x, HfO_2, ZrO_2, and Tm_2O_3 (Liu *et al* 2008; Yu *et al* 2008; Hou *et al* 2011; Pan *et al* 2012).

Figure 5 shows the endurance characteristic of the $Ag/ZnMn_2O_4/p^+$-Si device. The resistive switching can be repeated stably for over 100 times under bipolar resistive switching mode. The resistance values of the HRS and LRS distribute in a certain range after multiple current-voltage cycles, especially for the HRS. As can be seen, the resistance ratio between HRS and LRS is maintained at about 10^2 after successive resistive switching operation. The high HRS/LRS ratio of the present device is able to tolerance the scatterings of the resistance, and provide enough memory margins for sense amplifier design. The endurance measurement ensures that the resistive switching between ON and OFF states is highly controllable, reversible and reproducible. The endurance is much longer than that of the ZnO:Mg-based RRAM device in our previous report (Gao *et al* 2012).

Figure 6 shows the evolution of V_{set} and V_{reset} after 100 times resistive switching cycles. There is no conspicuous decay in both V_{set} and V_{reset}. However, the voltages have a slight shift along positive voltage direction.

Figure 7 shows the cumulative probabilities of the set and reset voltages. The set and reset voltages under the bipolar mode are distinguishable. During 100 times resistive switching cycles, the statistic distribution of the V_{set} and V_{reset} is very tight, and has a quite large safe set and reset voltage margin.

The retention time of the $Ag/ZnMn_2O_4/p^+$-Si device at the HRS and LRS is measured at a voltage of 0·1 V and room temperature as shown in figure 8. The LRS and HRS currents maintain at about $2{\cdot}1\times10^{-4}$ and $2{\cdot}3\times10^{-6}$A, respectively, for over 10^5 s without applying any power supply. The current ratio between HRS and LRS memory states is more

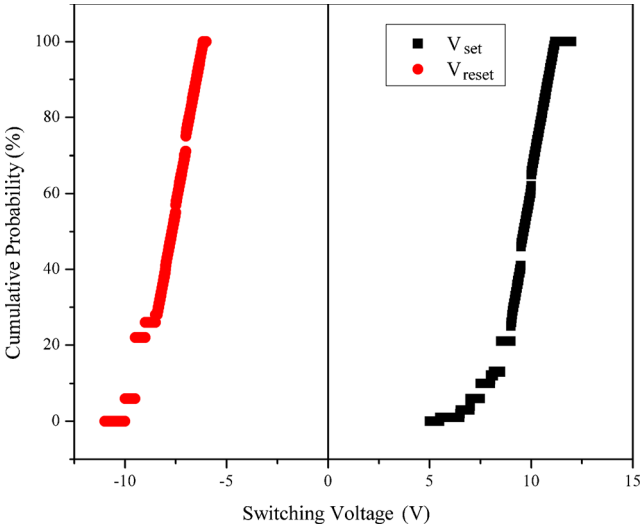

Figure 7. The cumulative probabilities of the set and reset voltages during the 100 resistive switching cycles.

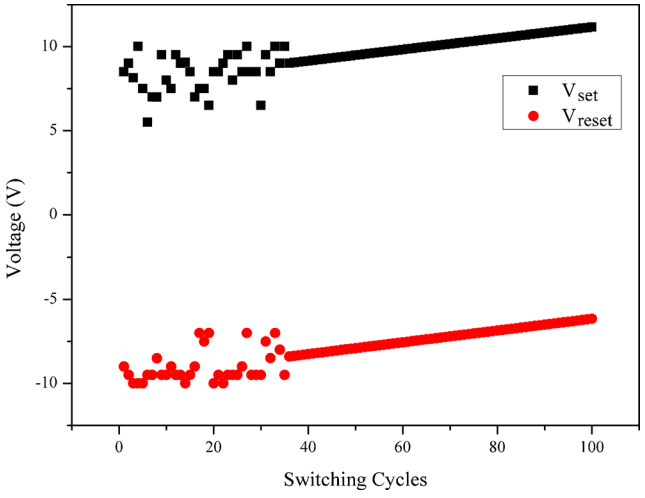

Figure 6. The evolution of the set and reset voltages during the 100 resistive switching cycles.

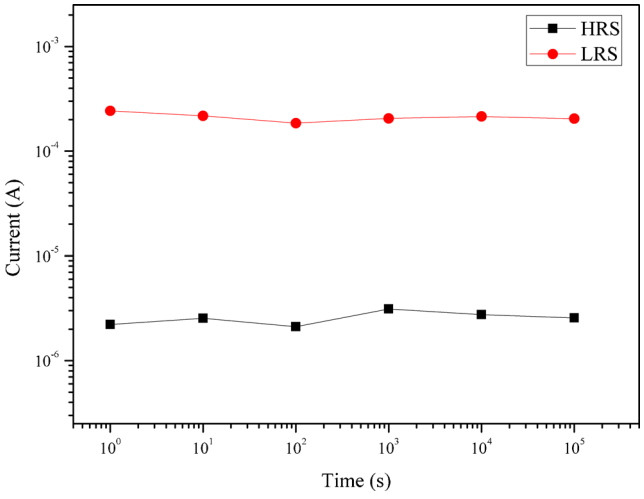

Figure 8. The retention-time test results of the HRS and LRS readout at 0·1 V.

than 10^2 times. Consequently, the good nonvolatility of the device is demonstrated.

4. Conclusions

The $ZnMn_2O_4$ resistive switching active layer with thickness of about 400 nm on p^+-Si substrate was fabricated by chemical solution deposition. The $ZnMn_2O_4$ active layer shows dense and crystallized structure with grain size of 30–90 nm. The Ag/$ZnMn_2O_4$/p^+-Si capacitor exhibits bipolar resistive switching behaviour. The memory states of the device can be set and reset between HRS and LRS by applying an external bias voltage. The device has reproducible bipolar resistive switching with high HRS/LRS ratio of $>10^2$ and long retention times of $>10^5$ s. The switching behaviour in LRS is dominated by the Ohmic behaviour, which suggests the filamentary conduction mechanism. However, the conduction behaviours in HRS successively undergo Ohm's law, trap-filled-limited and Child's law.

Acknowledgements

This research work was jointly sponsored by National Natural Science Foundation of China (Grant No. 61066001 and No.51262003) and Guangxi Key Laboratory of Information Materials (Guilin University of Electronic Technology), China (Project No. 1110908-10-Z).

References

Chang W Y, Lin C A, He J H and Wu T B 2010 *Appl. Phys. Lett.* **96** 242109

Chiu F C, Chou H W and Lee J Y 2005 *J. Appl. Phys.* **97** 103503

Chua L O 1971 *IEEE Trans. Circ. Theor.* **18** 507

Gao S M, Wang H, Xu J W, Yuan C L and Zhang X W 2012 *Solid-State Electron.* **76** 40

Hou T H, Lin K L, Shieh J, Lin J H, Chou C T and Lee Y J 2011 *Appl. Phys. Lett.* **98** 103511

Lin C C, Chang Y P, Ho C C, Shen Y S and Chiou B S 2011 *IEEE Trans. Magn.* **47** 633

Liu S Q, Wu N J and Ignatiev A 2000 *Appl. Phys. Lett.* **76** 2749

Liu Q, Guan W H, Long S B, Jia R and Liu M 2008 *Appl. Phys. Lett.* **92** 012117

Pan T M, Lu C H, Mondal S and Ko F H 2012 *IEEE Trans. Nanotechnol.* **11** 1040

Peng H Y and Wu T 2009 *Appl. Phys. Lett.* **95** 152106

Pradel A, Frolet N, Ramonda M, Piarristeguy A and Ribes M 2011 *Phys. Status Solidi. A* **208** 2303

Villafuerte M, Heluani S P, Juarez G, Simonelli G, Braunstein G and Duhalde S 2007 *Appl. Phys. Lett.* **90** 052105

Waser R and Aono M 2007 *Nat. Mater.* **6** 833

Yang Y C, Pan F, Liu Q, Liu M and Zeng F 2009 *Nano Lett.* **9** 1636

Yu L E, Kim S, Ryu M K, Choi S Y and Choi Y K 2008 *IEEE Electron. Dev. Lett.* **29** 331

Zhang S, Long S B, Guan W H, Liu Q, Wang W and Liu M 2009 *J. Phys. D: Appl. Phys.* **42** 055112